ehp ENVIRONMENTAL HEALTH PERSPECTIVES
http://www.ehponline.org

Persistent Organic Pollutants Modify Gut Microbiota–Host Metabolic Homeostasis in Mice Through Aryl Hydrocarbon Receptor Activation

Limin Zhang, Robert G. Nichols, Jared Correll, Iain A. Murray, Naoki Tanaka, Philip Smith, Troy D. Hubbard, Aswathy Sebastian, Istvan Albert, Emmanuel Hatzakis, Frank J. Gonzalez, Gary H. Perdew, and Andrew D. Patterson

http://dx.doi.org/10.1289/ehp.1409055

Received: 7 August 2014
Accepted: 9 March 2015
Advance Publication: 13 March 2015

Persistent Organic Pollutants Modify Gut Microbiota–Host Metabolic Homeostasis in Mice Through Aryl Hydrocarbon Receptor Activation

Limin Zhang,[1,2] Robert G. Nichols,[1] Jared Correll,[1] Iain A. Murray,[1] Naoki Tanaka,[3] Philip Smith,[1] Troy D. Hubbard,[1] Aswathy Sebastian,[4] Istvan Albert,[4] Emmanuel Hatzakis,[5] Frank J. Gonzalez,[3] Gary H. Perdew,[1] and Andrew D. Patterson[1]

[1]Center for Molecular Toxicology and Carcinogenesis, Department of Veterinary and Biomedical Sciences, The Pennsylvania State University, University Park, Pennsylvania, USA; [2]CAS Key Laboratory of Magnetic Resonance in Biological Systems, State Key Laboratory of Magnetic Resonance and Atomic and Molecular Physics, Wuhan Centre for Magnetic Resonance, Wuhan Institute of Physics and Mathematics, Chinese Academy of Sciences (CAS), Wuhan, China; [3]Laboratory of Metabolism, National Cancer Institute, National Institutes of Health, Bethesda, Maryland, USA; [4]Bioinformatics Consulting Center, The Pennsylvania State University, University Park, Pennsylvania, USA; [5]Department of Chemistry, The Pennsylvania State University, University Park, Pennsylvania, USA

Address correspondence to Andrew D. Patterson, Center for Molecular Toxicology and Carcinogenesis, Department of Veterinary and Biomedical Sciences, The Pennsylvania State University, University Park, PA 16801 USA. Telephone: 814-867-4565. E-mail: adp117@psu.edu

Running title: The impact of AHR activation on gut microbiota

Acknowledgments: This work was supported by National Institute of Environmental Health Sciences [Grants ES004869 (GHP), ES019964 (GHP), and ES022186 (ADP)] and by the Intramural Research Program of the Center for Cancer Research, National Cancer Institute, National Institutes of Health. Dr. Limin Zhang is a Penn State Institutes of Energy and the Environment Research Fellow.

Competing financial interests: All authors have no conflicts to declare.

Abstract

Background: Alteration of the gut microbiota through diet and environmental contaminants may disturb physiological homeostasis, leading to various diseases including obesity and type 2 diabetes. Since most exposure to environmentally-persistent organic pollutants (POPs) occurs through the diet, the host gastrointestinal tract and commensal gut microbiota are likely to be exposed to POPs.

Objectives: We report that 2,3,7,8-tetrachlorodibenzofuran (TCDF), a persistent environmental contaminant, profoundly impacts the gut microbiota and host metabolism in an aryl hydrocarbon receptor (AHR)-dependent manner.

Methods: Six-week-old male wild-type and *Ahr*$^{-/-}$ mice on the C57BL/6J background were treated with 24 μg/kg TCDF in the diet for five days. 16S rRNA gene sequencing, ^{1}H nuclear magnetic resonance (NMR) metabolomics, targeted ultra-performance liquid chromatography coupled with triplequadrupole mass spectrometry (UPLC-TQMS) and biochemical assays were used to determine the microbiota compositions and the physiological and metabolic effects of TCDF.

Results: Dietary TCDF altered the gut microbiota by shifting the ratio of *Firmicutes* to *Bacteroidetes*. TCDF-treated mouse cecal contents were enriched with *Butyrivibrio* spp., but depleted in *Oscillobacter* spp. in comparison with vehicle-treated mice. These changes in the gut microbiota were associated with altered bile acid metabolism. Further, dietary TCDF inhibited the farnesoid X receptor (FXR) signaling pathway, and triggered significant inflammation and host metabolic disorders as a result of activation of bacterial fermentation, and altering hepatic lipogenesis, gluconeogenesis and glycogenolysis, in an AHR-dependent manner.

Conclusion: These findings provide new insights into the biochemical consequences of TCDF exposure involving the alteration of the gut microbiota, modulation of nuclear receptor signaling, and disruption of host metabolism.

Introduction

Obesity risk factors include changes in diet and lifestyle and in some rare instances can be explained by genetic predisposition (Jaaskelainen et al. 2013); however these factors alone seem unlikely to explain the growing worldwide obesity epidemic. There is increasing evidence that chronic exposure to environmental chemicals through the diet, especially persistent organic pollutants (POPs), may promote the development of obesity and type 2 diabetes in humans (Lee et al. 2014). Of particular interest is the role of the aryl hydrocarbon receptor (AHR), which is bound and activated by a variety of POPs including coplanar polychlorinated biphenyls and halogenated aromatic hydrocarbons (HAHs), in mediating the toxic effects of these compounds at high doses (Alaluusua and Lukinmaa 2006; Ren et al. 2011) and promoting obesity at low doses (Arsenescu et al. 2008; Howell and Mangum 2011). More recent evidence suggests that the gut microbiota, which can be modulated by the AHR (Jin et al. 2014), may play a pivotal role in POP-induced obesity (Myre and Imbeault 2014).

The AHR is a xenobiotic sensor which was recently shown to be a pivotal regulator of gut and immune homeostasis (Monteleone et al. 2012). AHR agonists including both endogenous (e.g., several tryptophan catabolites), dietary (e.g., indole-3-carbinol metabolite indolo[3,2b] carbazole) and xenobiotic (e.g., 2,3,7,8-tetrachlorodibenzo-p-dioxin, TCDD) ligands can dramatically impact host metabolism and immunity (Bjeldanes et al. 1991; Claus et al. 2008; Michelle et al. 2013; Zelante et al. 2013). For example, microbiota-derived tryptophan metabolites including indole-3-aldehyde, were shown to modulate the AHR-IL-22 axis thus impacting mucosal immune homeostasis in the gut (Zelante et al. 2013). Furthermore, alteration of the gut microbiota through dietary manipulation and the presence of environmental contaminants may disturb physiological homeostasis leading to various diseases such as obesity (Greenblum et al.

2012), diabetes (Mathis and Benoist 2012) and inflammatory bowel disease (IBD) (Nagalingam and Lynch 2012). Recent studies suggest that interactions between the gut microbiota and environmental toxicants may contribute in part to the development of obesity and diabetes (Snedeker and Hay 2012). Therefore, bacteria in the gut may be impacted by dietary exposure to TCDD and other TCDD-like compounds thus altering not only bacterial populations but also their inherent metabolic activity (Maurice et al. 2013). In this study, TCDF was used instead of TCDD given its considerably shorter half-life in rodents (DeVito and Birnbaum 1995), yet was provided at doses higher than that typically found in the diet with polychlorinated dibenzo-*p*-dioxins and dibenzofurans for adults (0.3 to 3.0 pg TEQs/kg body weight) (Tadashi et al. 2011; Arnold et al. 1994). Further, TCDF was provided through the diet over five days as this represents the major route of exposure in humans (Jones and Bennett 1989).

Here, a combination of 16S rRNA metagenomics, metabolite profiling (ultraperformance liquid chromatography coupled with triplequadrupole mass spectrometry), and ^{1}H NMR-based metabolomics was used to investigate the alteration of the gut microbiota and host metabolome in mice treated with TCDF through the diet. In addition, possible correlations between the gut microbiota composition and signaling pathways such as AHR and FXR after TCDF exposure were investigated with the goal to identify a specific host-microbiota signaling axis. These findings provide new evidence that exposure to persistent environmental contaminants mediated through activation of the AHR strongly impacts the gut microbiota and host metabolism.

Materials and Methods

Animals and diets

Animal experimental procedures were performed according to the National Institutes of Health (NIH) guidelines and reviewed and approved by the Pennsylvania State University Institutional Animal Care and Use Committee. Mice were treated humanely and with regard for the alleviation of suffering. A total of 12 8-week-old male C57BL/6J mice were purchased from the Jackson Laboratory and housed together in groups of 2-4 mice per cage with a 12 h light/dark cycle at constant temperature (23 ± 1 °C) and humidity (45–65%) and allowed free access to food and water. Bedding material consisted of Alpha Dri (Shepherd Specialty Papers). After acclimatization for one week to normal flora in our facility, mice were randomly divided into two groups of six and trained to eat transgenic dough pills (Bio-Serve) without TCDF (Cambridge Isotope Laboratories, Inc.) for another four days. The dough pills containing TCDF (acetone solution as vehicle) were prepared with tablet molds and one pill uniformly contained 0.6 μg TCDF thus providing a final dose of 24 μg/kg. In the TCDF studies, mice were fed with the dough pills containing TCDF continuously for five days in the morning (one pill per mouse per day). Urine and feces were collected every other day (i.e., day 2, 4, and 6) over the TCDF treatment period. Blood, liver, intestine, cecum and cecal content samples were collected immediately following CO_2 asphyxiation on day 7. All samples were stored at -80°C until analysis. 10 male *Ahr*$^{-/-}$ mice (C57BL/6J congenic mice) were obtained from Dr. Christopher Bradfield (University of Wisconsin) and inbred to maintain the line. All mice were killed by CO_2 asphyxiation at 13:00 h after transporting to the laboratory.

Quantitative real-time PCR

RNA was extracted from frozen liver and intestine (~50 mg) using TRIzol reagent (Invitrogen). cDNA was synthesized from 1 μg of total RNA using Superscript II reverse transcriptase (Invitrogen) and the products were diluted to 1:10 before use in subsequent reactions. Gene-specific primers were used in each reaction and all results were normalized to the ribosomal protein *L13* or *β-actin* mRNA (primer sequences can be found in Supplemental Material Table S1). QPCR assays were carried out using SYBR green QPCR master mix on an ABI Prism 7900HT Fast Real-Time PCR sequence detection system (Applied Biosystems). The reactions were analyzed according to the ΔΔCT method. QPCR conditions were 40 cycles of 95°C for 20 s; 95 °C for 0.01 s; 60 °C for 20 s; 95 °C for 15 s; 60 °C for 15 s and 95 °C for 15 s.

16S rRNA gene sequencing of the microbiota

The bacteria in the cecal contents were extracted using the PowerSoil DNA Isolation Kit (Mo Bio laboratory, Inc.). The PCR products (~1,000 bp) were purified using the Agencourt AMPure technology (Beckman Coulter) as described in 454 Technical Bulletin number 2011-002, Short Fragment Removal Procedure. After purification, the products were quantified by both Qubit (Lifetech, Carlsbad, CA) and qPCR, using the KAPA Biosystems Library Quantification Kit (Kapa-Biosystems). Products were pooled based on molar amounts, subjected to electrophoresis on a 1% agarose gel and extracted. After purification with a QIAquick PCR Purification kit (Qiagen), the quality and quantity of the preparations were assessed using a DNA 7500LabChip on the Agilent 2100 Bioanalyzer (Agilent Technologies) and Qubit quantification. Sequencing was performed using a quarter Picotiter Plate on a 454 Life Sciences Genome Sequencer FLX (Roche Diagnostics). 16S rRNA gene sequencing analysis was done using the mothur platform as previously described (Schloss et al. 2009).

Bile acid profiling by triplequadrupole mass spectrometry

Targeted analysis of bile acids was performed using an Acquity UPLC system coupled to a Waters Xevo TQS MS (Waters) with a C18 BEH (2.1x100 mm, 1.7 µm) column (Waters). External bile acid standards including cholic acid (CA), lithocholic acid (LCA), chenodeoxycholic acid (CDCA), deoxycholic acid (DCA), ursodeoxycholic acid (UDCA), α-muricholic acid (αMCA), β-muricholic acid (βMCA), ω-muricholic acid (ωMCA), glycocholic acid (GCA), glycochenodeoxycholic acid (GCDCA), taurocholic acid (TCA), taurodeoxycholic acid (TDCA), tauro chenodeoxycholic acid (TCDCA), taurolithocholic acid (TLCA), tauro-α-muricholic acid (TαMCA) and tauro-β-muricholic acid (TβMCA) were purchased from Sigma-Aldrich (St. Louis, MO). The deuterated internal standards cholic acid-2,2,4,4-D4 (CA-d4), lithocholic acid-2,2,4,4-D4 (LCA-d4), ursodeoxycholic acid-2,2,4,4-D4 (UDCA-d4), chenodeoxycholic acid-2,2,4,4 (CDCA-d4), and deoxycholic acid-2,2,4,4-D4 (DCA-d4) were obtained from Sigma-Aldrich. Tissues and feces were weighed (25 mg) and internal standards (5 µL, 1 µg/mL) were added before extraction with 500 µL ethanol by homogenization followed by shaking at 60°C for 30 min. After cooling, the samples were incubated at 100°C for 3 minutes and centrifuged at 1600 x g for 10 min at 4°C and supernatants were transferred to a new tube. The pellets were extracted twice with 500 µL ethanol. After centrifugation at 11200 x g for 1 min at 4°C, the combined supernatants were dried down and later dissolved with 500 µL methanol. Following vortexing and centrifugation, 300 µL of the supernatant was transferred to an autosampler vial. Analytes were detected by selected ion monitoring (SIM) or multiple reaction monitoring (MRM) and normalized by internal standard. Analytes of CA, LCA, UDCA, CDCA, and DCA were quantified with their respective deuterated internal standards. Others were quantified with CA-d4. The results were calculated according to individual standard curves

established with the response ($area_{analyte}/area_{internal\ std.}$). Retention times of analytes and their SIM/MRM are presented in Supplemental Material Table S2.

Fecal IgA and serum LAL measurements

IgA mouse enzyme-linked immunosorbent assay (ELISA) kits, Pierce LAL chromogenic endotoxin quantitation kits and Lipocalin-2 (LCN2) ELISA kits were purchased from Abcam and Thermo Scientific, respectively. Fecal IgA, LCN2 and serum LAL were measured according to vendor instructions.

Scanning electron microscopy

Scanning electron microscopy (SEM) images were used for observation of the gut microbiota morphology particularly to visualize bacteria associated with the intestinal epithelium. The ileum was opened and fixed with 2% glutaraldehyde overnight at 4°C. Samples were washed with 0.1 M sodium cacodylate buffer pH 7.4 three times and then post fixed with 1% osmium tetroxide in 0.1 M sodium cacodylate buffer. The samples were washed and dehydrated through a graded ethanol series then critical point dried, mounted and coated with 10 nm Au/Pd. Images were acquired on a JEOL JSM 5400 SEM.

TCDF reporter assay

TCDF treatment in *Ahr*$^{-/-}$ mice was confirmed with the Hepa1.1 mouse hepatoma reporter cell line. After killing the *Ahr*$^{-/-}$ mice, 50 mg of liver was extracted using the Folch method (Folch et al. 1957), lyophylized, and reconstituted in 20 µL of DMSO and 0.1 µL of the DMSO reconstituted extracted was used for the reporter assay. The Hepa 1.1 mouse hepatoma cell line containing the stably integrated pGudluc 1.1 luciferase reporter construct was obtained from Dr. Michael Denison (University of California, Davis, CA). The Hepa 1.1 mouse hepatoma cell line

was maintained in α-modified essential media (Sigma-Aldrich) supplemented with 8% fetal bovine serum (Hyclone Laboratories), 100 IU/ml penicillin/100 μg/ml streptomycin (Sigma-Aldrich). Cells were cultured at 37°C in a humidified atmosphere composed of 95% air and 5% CO_2. The reporter cells (Hepa 1.1) were seeded in twelve-well plates and cultured to ~90% confluence. The AHR-responsiveness of extracts was examined after treatment for 4 h followed by lysing with 400 μL of lysis buffer.

Histopathology and clinical biochemistry

Formalin fixed liver tissue was embedded in paraffin wax, sectioned (3-4 μm), and stained with hematoxylin and eosin (H&E) followed by examination under a microscope by a qualified liver pathologist (Dr. Naoki Tanaka, NCI, NIH). Serum alanine transaminase (ALT) and alkaline phosphatase (ALP) were measured with VetScan VS2 using the Mammalian Liver Profile disk (Abaxis) according to vendor instructions.

NMR-based metabolomics experiment

Sample preparation

Liver and intestinal tissues (~50 mg) were extracted three times with 600 μL of precooled methanol-water mixture (2/1, v/v) using the PreCellys Tissue Homogenizer (Bertin Technologies, Rockville, MD). Fecal and cecal content samples (~50 mg) were subjected to three consecutive freeze-thaws and directly extracted by precooled phosphate buffer with homogenization using the Precellys Tissue Homogenizer. After extraction, 550 μL of each extract was centrifuged and then transferred to a 5 mm NMR tube (for more detailed methods, see Supplemental Material, NMR-Based Metabolomics, sample preparation).

^{1}H NMR spectroscopy

^{1}H NMR spectra of all the biological samples were recorded at 298 K on a Bruker Avance III 600 MHz spectrometer (operating at 600.08 MHz for ^{1}H) equipped with a Bruker inverse cryogenic probe (Bruker Biospin). Typical one-dimensional NMR spectra were acquired for each of the samples employing the first increment of NOESY pulse sequence (NOESYPR1D). To facilitate NMR signal assignments, a range of 2D NMR spectra were acquired and processed for selected samples (for more detailed methods, see Supplemental Material, NMR-Based Metabolomics, ^{1}H NMR Spectroscopy).

NMR data processing and multivariate data analysis

^{1}H NMR spectra were corrected manually for phase and baseline distortions and spectral region δ 0.5-9.5 was integrated into regions with equal width of 0.004 ppm (2.4 Hz) using AMIX software package (V3.8, Bruker-Biospin, Germany). Multivariate data analyses including Principal Component Analysis (PCA) and Orthogonal Projection to Latent Structures with Discriminant Analysis (OPLS-DA) were carried out on the NMR data with SIMCAP+ software (version 13.0, Umetrics, Sweden). To facilitate interpretation of the results, color-coded correlation coefficients plots were performed with back-transformation of the loadings generated from the OPLS-DA using an in-house developed script for MATLAB (The Mathworks Inc.; Natwick, MA) (see Supplemental Material, NMR-Based Metabolomics, Spectral Data Processing and Multivariate Data Analysis).

Data analysis

All the experimental values are presented as mean ± s.d. Graphical illustrations and statistical analysis were performed with GraphPad Prism version 6.0 (GraphPad). *P*-values < 0.05 were considered as significant.

Results

Effects of dietary TCDF on liver enzymes and morphology

The effect of sustained AHR activation on the gut was assessed using a potent AHR ligand, TCDF. $Ahr^{+/+}$ and $Ahr^{-/-}$ mice treated with dietary TCDF (24 µg/kg body weight) exhibited mild and no histopathological changes in the liver, respectively (Figure 1A and B). Mildly elevated serum ALT (19.3 - 37.5 U/L) and ALP (36.5 - 52.2 U/L) levels (Figure 1C) and no significant differences in body weight (Figure 1D) were observed in the $Ahr^{+/+}$ mice after TCDF treatment thus indicating minimal hepatic toxicity. Further, no evidence of steatosis, bile duct injury, or cellular degeneration was found as is often observed with high dose TCDD treatment (Ozeki et al. 2011). $Ahr^{-/-}$ mice exhibited no significant changes in the liver enzymes ALT and ALP (Figure 1C). TCDF exposure in the $Ahr^{-/-}$ mice was confirmed using dichloromethane extracts of liver and assessing the induction of AHR signaling in a Hepa 1.1 stable reporter line (see Supplemental Material, Figure S1). Transcriptional targets of AHR including *Cyp1a1*, *Cyp1a2* and *Cyp2e1* were significantly induced in the liver and across the small intestine (Figure 1E) and were AHR dependent (Figure 1F). These observations suggest that the subsequent metabolic changes described below were specific to AHR activation and not due to overt liver toxicity.

Effects of dietary TCDF on the morphology, population and composition of the gut microbiota

Given recent evidence that the AHR is important for regulating gut homeostasis (Monteleone et al. 2013), changes in the gut microbiota upon oral dietary exposure to POPs were examined (Snedeker and Hay 2012). Weighted UniFrac principal coordinate analyses (for assessing changes in abundance) of 16S rRNA sequencing results indicated that dietary TCDF induced a remarkable change in the overall gut microbiota population (Figure 2A). *Firmicutes* and *Bacteroidetes* exhibited significant changes with reduction of *Firmicutes*/*Bacteroidetes* ratio after dietary TCDF exposure (Figure 2B, see Supplemental Material Figure S2A-D). Furthermore, TCDF-treated mouse cecal contents were enriched with *Butyrivibrio* spp., but depleted in *Oscillobacter* spp. in comparison with the vehicle-treated mice (Figure 2C). Further an increase in the class *Flavobacteria* but a decrease in the class *Clostridia* was observed. Scanning electron microscope (SEM) images showed that dense segmented filamentous bacteria (SFB) form a network of segmented filaments in the ileum of vehicle-treated mice, whereas they were dramatically depleted in the ileum of TCDF-treated mice (Figure 2D). Quantitative real-time PCR (QPCR) analyses revealed that dietary TCDF significantly reduced SFB levles in the ileum with no significant changes observed between TCDF-treated *Ahr*$^{-/-}$ mice and vehicle-treated *Ahr*$^{-/-}$ mice (Figure 2E).

Inflammatory signaling and immune responses

TCDF led to a significant increase in mRNAs encoding factors in the ileum involved in inflammatory signaling, such as *Il-1β*, *Il-10*, *Tnf-α*, *Saa1* and *Saa3* (Figure 3A); these changes were AHR-dependent (Figure 3B). *Lcn-2* mRNA, encoding lipocalin-2, a sensitive biomarker for intestinal inflammation (Chassaing et al. 2012), was dramatically increased in the ileum (Figure

3C, left) and in the feces (Figure 3D) of mice exposed to TCDF. No significant change in *Lcn-2* mRNA (Figure 3C, right) was observed in the ileum of *Ahr*$^{-/-}$ mice after TCDF-treatment. Dietary TCDF caused a significant elevation of serum lipopolysaccharide (LPS) (Figure 3F) and fecal immunoglobulin A (IgA) (Figure 3G), and depleted of *Myosin Vb* and *Ptprh* in the ileum tissue (Figure 3E), which are closely associated with gut permeability and the host immune system. Taken together, these results suggest that dietary TCDF triggers robust intestinal inflammation and inflammatory signaling in mice in an AHR-dependent manner.

Bile acid metabolism

It is well known that the gut microbiota have profound effects on bile acid metabolism (Nicholson et al. 2012). To determine whether the composition of bile acids was affected by dietary TCDF exposure, ultra-performance liquid chromatography coupled with triple quadrupole tandem mass spectrometry (UPLC-TQMS) was employed to examine the bile acid composition and their levels in the liver, intestine, cecum, and feces according to published methods (Jiang et al. 2015). Compared with vehicle-treated mice, TCDF-treated mice contained significantly higher levels of DCA in the small intestine and feces (Figure 4A and 4C) and three conjugated bile acids (GCA, TCDCA and TβMCA) (Figure 4B and 4D) that were affected by gut microbial metabolism as previously reported (Sayin et al. 2013). The size of the bile acid pool was found to be significantly increased in the TCDF-treated mice (Figure 4E). In addition, levels of LCA (intestine and cecum), CDCA (liver) and TLCA (liver and feces) in TCDF-treated mice were higher than those in vehicle-treated mice (see Supplemental Material, Figure S3A-E).

Effects of dietary TCDF on gene expression profiles and FXR signaling

FXR serves as a critical modulator of enterohepatic circulation and thus plays a key role in the regulation of bile acid synthesis and homeostasis (Claudel et al. 2005). TCDF treatment was associated with significant down-regulation of *Fxr* mRNA and its target gene small heterodimer partner (*Shp*) mRNA in both the ileum and liver of mice (Figure 4F and 4G). Intestinal fibroblast growth factor 15 (*Fgf15*) mRNA, which encodes a growth factor that is released by small intestine epithelial cells, which was also markedly decreased by TCDF treatment (Figure 4F). In addition, no significant differences in the expression of *Fxr*, *Fgf15* and *Shp* in the ileum (Figure 4F) or liver (Figure 4G) were observed between TCDF-treated $Ahr^{-/-}$ mice and vehicle-treated $Ahr^{-/-}$ mice. Taken together, these observations indicate that TCDF impacts the FXR signaling pathways through an AHR-dependent mechanism.

Effects of dietary TCDF on gene expression profiles: genes associated with bile acid synthesis, conjugation and reabsorption

Next, the question of whether altered bile acid profiles in TCDF-treated mice was associated with changes in gene expression of enzymes involved in bile acid synthesis and/or transport were addressed. TCDF treatment resulted in a 10-fold elevation in the expression of *Cyp7a1* mRNA in the liver (Figure 4H) and CYP7A1 protein levels were also increased (see Supplemental Material, Figure S4). Expression of *Cyp7b1* mRNA was also increased by 1.8-fold in the liver (Figure 4H). In contrast, no significant change in *Cyp7a1* mRNA expression was observed upon treatment of $Ahr^{-/-}$ mice with TCDF (see Supplemental Material, Figure S3E). The expression of mRNAs encoded by other genes such as *Cyp8b1*, *Cyp27a1* and *Akr1d1*, all involved in bile acid synthesis, were not significantly affected by TCDF exposure (Figure 4H).

A significant decrease in mRNAs encoding the taurine biosynthetic enzymes, cysteine dioxygenase (CDO) and cysteine sulfinate decarboxylase (CSD), the rate-limiting enzyme for the conversion of cysteine to taurine (Bitoun and Tappaz 2000a, b), were found in the livers of TCDF-treated mice (Figure 4I). These observations were confirmed with the TCDF-induced down-regulation of taurine levels in gut tissues as revealed by ^{1}H NMR metabolomics (see Supplemental Material, Figure S6A-C; see Supplemental Material, Table S3). However, expression of the taurine transporter (*Taut*) mRNA, the main regulator of intracellular taurine levels (Bitoun and Tappaz 2000b), was up-regulated in the livers of TCDF-treated mice (Figure 4I), which may indicate an attempt to compensate for the reduced hepatic taurine content. A significant elevation in the expression of bile acid-CoA synthetase (*Bacs*) mRNA, encoding an important enzyme involved in the process of bile acid conjugation with taurine, in the livers of TCDF-treated mice was also noted (Figure 4I). These results are in agreement with the observation of elevated taurine-conjugated bile acids.

For enterohepatic circulation of bile acids, both the hepatocyte and the enterocyte must efficiently transport bile acids. Thus, transporters play key roles for the transport and reabsorption of bile acids. Here, the expression of genes involved in bile acid transport and homeostasis in liver and ileum were determined (Figure 4J-K). Multidrug-resistance protein (*Mrp3*) gene was significantly up-regulated in the livers of TCDF-treated mice (Figure 4J). Previous studies reported that TCDD exposure resulted in up-regulation of *Mrp3*, in mouse liver (Maher et al. 2005) and induced expression of inflammatory mediators, as well as necrosis and/or apoptosis related genes (Hayashi et al. 2005). Expression of *Mrp2* and *Ibat* mRNAs encoding apical bile acid transporters, were down-regulated whereas *Mrp3* mRNA, encoding one

of the basolateral bile acid transports, was up-regulated in the ileum of TCDF-treated mice (Figure 4K).

Effects of dietary TCDF on the host metabolome

^{1}H-NMR-based metabolomics coupled with multivariate statistical analysis was employed to evaluate the metabolic changes induced by TCDF exposure. Typical ^{1}H-NMR spectra of liver, fecal, and cecal content extracts obtained from vehicle- and TCDF-treated mice are shown (see Supplemental Material, Figure S5A-F). Metabolite assignments were carried out as described earlier (Tian et al. 2012; Wu et al. 2010) and confirmed with a series of two-dimensional (2D) NMR experiments (see Supplemental Material, Table S4). In order to obtain the metabolic variations associated with different biological sample groups, pair-wise OPLS-DA was performed between data obtained from feces (Figure 5A), cecal contents (Figure 5B), liver (Figure 5C), and gut tissues including duodenum, jejunum, ileum, and cecum (see Supplemental Material, Figure S6A-D) of mice from vehicle and TCDF-treated groups. The model quality indicators (R^2X and Q^2, see Supplemental Material, Table S3) clearly showed that the extracts obtained from the biological matrices were distinctive in terms of their metabolite profiles. However, the Q^2 values (0.007, -0.12 and 0.29 for the models of feces, cecal contents and liver samples, respectively) of the OPLS-DA models of data from feces and cecal contents of *Ahr*$^{-/-}$ mice revealed no significant differences between the TCDF-treated and control *Ahr*$^{-/-}$ mice (see Supplemental Material, Figure S6E-G, Table S5). These observations were further supported by results from the model evaluation with CV-ANOVA ($p < 0.05$) and permutation test for the OPLS-DA models (see Supplemental Material, Table S5 and Figure S7). The metabolites with statistically significant contributions between TCDF-treated and vehicle-treated groups are identified in the corresponding color-coded coefficient plots (Figure 5A-C, see Supplemental

Material, Figure S6A-D) and the correlation coefficient values were also tabulated (see Supplemental Material, Table S3). Compared with the vehicle-treated mice, dietary TCDF significantly elevated the levels of short chain fatty acids (SCFAs) propionate and n-butyrate, but significantly decreased the levels of oligosaccharides and glucose in the feces and cecal contents (Figure 5A and B, see Supplemental Material, Table S3). Reliable assignments of n-butyrate and propionate were further confirmed by 2D ^{1}H-^{1}H TOCSY NMR spectroscopy (see Supplemental Material, Figure S8). Similar changes in SCFAs and oligosaccharides were also obtained from calculation of their relative concentration from the NMR peaks integration to internal standard (TSP) in feces and cecal contents of the TCDF-treated wild-type mice against those from the respective controls (see Supplemental Material, Figure S9A and B). However, no significant differences in the levels of SCFAs and oligosaccharides were observed in feces and cecal content between TCDF-treated and vehicle-treated *Ahr*$^{-/-}$ mice (see Supplemental Material, Figure S9A and B), supporting the dependence on AHR status. Significant increases in the expression of the G-protein coupled receptors (*Gpr41* and *Gpr43*), were found in the colons of TCDF-treated mice (see Supplemental Material, Figure S10A).

Dietary TCDF significantly elevated the levels of lipid, unsaturated fatty acid (UFA), and glycogen in the livers, and significantly decreased the levels of glucose, lactate, fumarate, a range of amino acids, nucleotide metabolites (e.g., inosine and hypoxanthine), nicotinurate, and cell membrane related metabolites (choline, PC, and GPC) in comparison with the vehicle-treated mice (Figure 5C). However, no significant change in lipid and glucose metabolism was observed in the liver of *Ahr*$^{-/-}$ mice after TCDF-treatment (see Supplemental Material, Figure S6G). Down-regulation of *Gck*, *G6pase*, *Glut2* and *Pepck* expression was found in the livers of TCDF-treated *Ahr*$^{+/+}$ mice (see Supplemental Material, Figure S10B).

In addition, dietary TCDF was also found to cause a significant elevation of amino acids including branched chain amino acids (leucine, isoleucine and valine), lysine, glutamine, tyrosine and phenylalanine, but reduction of taurine, choline, PC, GPC and some nucleic acids such as hypoxanthine and uridine in gut tissues (see Supplemental Material, Figure S6A-D, Table S3).

Discussion

Historically, POPs have been studied for their ability to cause adverse effects including liver toxicity (Lee et al. 2014). It is anticipated, however, that since most exposure to POPs occurs through the diet, the host gastrointestinal tract and gut microbiota are likely to be exposed to and modulated by POPs. Here TCDF treatment increased gut inflammation, modulated the gut microbiota population, increased bacterial fermentation, and had a profound impact on host metabolism in an AHR-dependent manner.

Based on allometric scaling calculations, the TCDF dose (24 μg/kg body weight) used in this study is equivalent to approximately 3000 ng/kg body weight in humans. Several epidemiological studies have reported that TCDD blood levels were on average 1434 ng/kg (range 301-3683 ng/kg) among workers involved in the remediation of the 2,4,5-trichlorophenol reactor accident in Seveso, Italy (WHO Consultation 1998). Accounting for the reduced toxicity of TCDF compared with TCDD (the TEF for TCDF is 0.1), the dose used in the present study is considerably higher than the estimated daily oral intake of polychlorinated dibenzo-*p*-dioxins and dibenzofurans for adults (0.3 to 3.0 pg TEQs/kg body weight) (Tadashi et al. 2011; Arnold et al. 1994). Furthermore, we have not accounted for total body burden and as mentioned above the absorbed TCDF dose is considerably higher than what is to be expected from normal dietary

intakes. However, the current study reinforces the idea that the gut microbiota are important targets and/or mediators of the toxicologic response and helps to establish possible endpoints for studies at lower doses.

One of the most prominent findings in the current investigation was the significant alteration of the gut microbiota by TCDF and changes in co-metabolites of the host and gut microbiota including bile acids and SCFAs. Within the intestinal microbiota, at the phylum level, TCDF treatment significantly shifted the microbial community from *Firmicutes* towards *Bacteroidetes*, indicating that the total population of the gut microbiota was modulated by TCDF. Similar observations were observed with oral exposure to PCB in mice, which interestingly, can be reversed with voluntary exercise (Choi et al. 2013). The predominant members, *Firmicutes* and *Bacteroidetes*, are known to provide key metabolic functions to their host (Hooper et al. 2002), as well as important developmental (Stappenbeck et al. 2002) and immunologic properties (Hooper et al. 2003; Mazmanian et al. 2005). Further, TCDF treatment enriched *Butyrivibrio* spp., common butyrate producing gut microbes, that are able to ferment a wide range of sugars and cellodextrins (Russell et al. 1985). The increased levels of *Butyrivibrio* spp. was confirmed with the activation of fermentation by TCDF treatment which induced significant depletion of glucose and oligosaccharides coupled with elevation of SCFAs such as butyrate and propionate in feces and cecal contents. Interestingly, certain members of the class *Flavobacteria* which includes *Flavobacterium* spp. were reported to possess dehalogenase activity and while it has not been demonstrated in isolates derived from the mammalian gut, they may contribute to the metabolism of TCDF and other halogenated compounds (Xun et al. 1992). A clear role for *Oscillibacter* spp. has not been established, but was reported to be associated with the development of fatty liver, an effect observed with TCDD exposure (Angrish et al. 2013;

Matsubara et al. 2012). Members of the *Clostridia* class and *Lactobacillus* spp. were reported to be associated with strong bile salt hydrolase (BSH) enzymatic activity (Li et al. 2013) and the elevation of deoxycholic acid (DCA), α-muricholic acid (αMCA) and taurine conjugated β-muricholic acid (TβMCA) suggest TCDF remodeling of gut microbiota contributes to changes in bile acid pools in the gut and liver (-Jin et al. 2014).

It should be noted that SFB (after mice were acclimated to our facility) were drastically depleted after TCDF treatment thus providing further evidence that TCDF impacted the gut microbiota. One of the most outstanding features of SFB as commensal bacteria is its specific attachment with host epithelial cells in the terminal ileum (Michele et al. 2010). Previous studies demonstrated that SFB were present only in mice that had Th17 cell-inducing microbiota which contain relatively abundant $CD4^+$, $IFN\gamma^+$ and $CD25^+Foxp3^+$ cells (Ivanov et al. 2009). SFB leads to an increase in the relative proportions of Th17 cells and Th17 cell cytokines which provide protection against mucosal infection through modulation of the immune response of the host. Furthermore, other high-affinity ligands of AHR, TCDD and 6-formylindolo [3, 2-b] carbazole (FICZ) were shown to correlate with an increased frequency of Th17 cells (Hautekiet et al. 2008; Marshall and Kerkvliet 2010). Thus, TCDF exposure may be associated with heightened immune response that is dependent on AHR status. Additional studies focused on the direct impact of TCDF and other POPs on the gut microbiota are indeed warranted and should shed some light on how these compounds might influence the gut microbiota population directly.

Supporting the overall assertion that dietary TCDF exposure leads to a broad inflammatory response in mice is the significant elevation of fecal IgA, fecal LCN-2, serum LPS and mRNA expression of intestinal innate immune factors including, *Il-1β*, *Il-10*, *Tnf-α*, *Saa1* and *Saa3*

reported here. One possible explanation for these results is that the AHR plays a direct role in the regulation of inflammatory gene expression. There is support for this notion through recent studies that found functional dioxin response elements in the *Il-6* promoter that are capable of synergistically increasing transcription in the presence of an inflammatory signal and an AHR ligand (DiNatale et al. 2010). The binding of the AHR to the *Il-6* promoter results in jettison of HDAC1 from the promoter leading to increased NF-kB occupation and acetylation. Whether the same type of combinatorial regulation occurs on other inflammatory genes remains to be explored. IgA, a major class of immunoglobulin, is produced in mucosal tissues and was shown to reduce intestinal proinflammatory signaling and bacterial epitope expression when binding to the commensal *Bacteroides thetaiotaomicron* (Peterson et al. 2007). This suggests that IgA inhibits innate immune responses and regulates the composition and the function of gut microbiota (Macpherson et al. 2012). LPS is found in the outer membrane of Gram-negative bacteria, contributes greatly to the structural integrity of the bacteria, acts as an endotoxin, and elicits strong immune responses in animals. LPS can mediate an *IL-10*-dependent inhibition of CD4 T-cell expansion and function by up-regulating PD-1 levels on monocytes, which leads to IL-10 production by monocytes after binding of PD-1 by PD-L (Said et al. 2010). Previous studies have shown that LPS in the portal vein or translocation of bacteria promotes intestinal fibrogenesis via TLR4, predominantly from gram-negative bacteria (Chan et al. 1997; Lin et al. 1995). In the current study, an elevated level of serum LPS would suggest an increase in gut permeability or altered immune surveillance leading to higher levels of inflammatory signaling in the TCDF-treated mice compared with the vehicle-treated mice. In addition, levels of LCN-2 a sensitive and dynamic non-invasive biomarker for intestinal inflammation, are dramatically increased upon TCDF exposure (Chassaing et al. 2012). It is important to note that, the observed

innate immune responses in mice induced by TCDF required AHR expression. Whether the heightened host inflammatory signaling observed through potent AHR activation leads to changes in the gut microbiota, which in turn causes additional alterations in gut homeostasis, remains to be investigated.

Another prominent finding of the present study was the profound changes of the host metabolome induced by TCDF. Particularly, TCDF induced significant reduction of glucose and oligosaccharides with elevation of SCFAs such as n-butyrate and propionate in feces and cecal content extracts indicating activation of bacterial fermentation by TCDF. SCFAs are clearly one of the most important gut microbial products and affect a range of host processes including energy utilization, host-microbe signaling, gut composition, and motility (Nicholson et al. 2012). Recently, it was shown that obesity is linked to the composition of human microbiota and the production of SCFAs providing an additional source of energy for the body (Schwiertz et al. 2010). In addition to being energy sources, SCFAs control colonic gene expression by inhibiting the enzyme histone deacetylase (HDAC) and metabolic regulation by signaling through G-protein-coupled receptors (GPCRs), such as GPR41 and GPR43 (Tremaroli and Backhed 2012). Significant elevation of colonic *Gpr41* and *Gpr43* mRNAs further indicated activation of bacterial fermentation by TCDF.

Significantly elevated levels of lipid and UFA in the liver of TCDF-treated mice indicate hepatic lipogenesis which appears to be a common cellular response to a number of liver toxic compounds such as allyl formate (Yap et al. 2006), acetaminophen (Coen et al. 2003), and aflatoxin-B1 (Zhang et al. 2011). Further, depletion of hepatic glucose and lactate coupled with elevation of glycogen in TCDF-treated mice (Figure 5) suggested that one of the consequences

of TCDF exposure is inhibition of gluconeogenesis and glycogenolysis. Similar observations were reported in the case of suppression of hepatic gluconeogenesis by TCDD through the AHR target gene *TiPARP* (Diani-Moore et al. 2010). Consistently, markedly decreased expression and activity of *Pepck*, *Gck*, *G6pase*, and *Glut2*, enzymes controlling gluconeogenic flux in the liver of TCDF-treated mice were also observed in this study. Interestingly TCDF exposure influences the FXR signaling pathway but the connection with AHR remains unclear. Further studies using tissue-specific *Ahr* knockout mice should yield important insights into how AHR status in different tissues (e.g., liver or intestinal epithelium) impacts the gut microbiota.

Conclusions

In summary, dietary TCDF induced alterations in the gut microbiota accompanied by modulation of bile acid metabolism and host immune responses. Depletion of *Clostridia* by TCDF was associated with accumulation of DCA that is involved in liver cancer (Shin et al. 2013). The increased TCDCA and TβMCA by TCDF were found to be associated with the inhibition of FXR signaling pathway. Furthermore, through activation ofAHR signaling, dietary TCDF altered many host metabolic pathways involving in hepatic lipogenesis, gluconeogenesis and glycogenolysis, bacteria fermentation and amino acids and nucleic acids metabolism. These findings provided new evidence that exposure to persistent environmental contaminants strongly impacts the gut microbiota-host metabolic axis in mice.

References

Alaluusua S, Lukinmaa PL. 2006. Developmental dental toxicity of dioxin and relatedcompounds-a review. Int J Dent 56:323-331.

Angrish MM, Dominici CY, Zacharewski TR. 2013. TCDD-elicited effects on liver, serum, and adipose lipid composition in C57BL/6 mice. Toxicol Sci 131:108-115.

Arnold S, James S. Christopher W, Mithell K, Olaf P, Anton L, Michael B,James RO.1994. Congener-specific levels of dioxins and dibenzofuransin U.S. food and estimated daily dioxin toxic equivalent intake. Environ Health Perspect 102:962-966.

Arsenescu V, Arsenescu RI, King V, Swanson H, Cassis LA. 2008. Polychlorinated biphenyl-77 induces adipocyte differentiation and proinflammatory adipokines and promotes obesity and atherosclerosis. Environ Health Perspect 116:761-768.

Bitoun M, Tappaz M. 2000a. Gene expression of taurine transporter and taurine biosynthetic enzymes in brain of rats with acute or chronic hyperosmotic plasma. A comparative study with gene expression of myo-inositol transporter, betaine transporter and sorbitol biosynthetic enzyme. Brain Res 77:10-18.

Bitoun M, Tappaz M. 2000b. Gene expression of taurine transporter and taurine biosynthetic enzymes in hyperosmotic states: a comparative study with the expression of the genes involved in the accumulation of other osmolytes. Adv Exp Med Biol 483:239-248.

Bjeldanes LF, Kim JY, Grose KR, Bartholomew JC, Bradfield CA. 1991. Aromatic hydrocarbon responsiveness-receptor agonists generated from indole-3-carbinol in vitro and in vivo: comparisons with 2,3,7,8-tetrachlorodibenzo-p-dioxin. Proc Natl Acad Sci USA 88:9543-9547.

Chan CC, Hwang SJ, Lee FY, Wang SS, Chang FY, Li CP et al. 1997. Prognostic value of plasma endotoxin levels in patients with cirrhosis. Scand J Gastroentero 32:942-946.

Chassaing B, Srinivasan G, Delgado MA, Young AN, Gewirtz AT, Vijay-Kumar M. 2012. Fecal lipocalin 2, a sensitive and broadly dynamic non-invasive biomarker for intestinal inflammation. PloS one 7: e44328.

Choi JJ, Eum SY, Rampersaud E, Daunert S, Abreu MT, Toborek M. 2013. Exercise attenuates PCB-induced changes in the mouse gut microbiome. Environ Health Perspect 121:725-730.

Claudel T, Staels B, Kuipers F. 2005. The Farnesoid X receptor: a molecular link between bile acid and lipid and glucose metabolism. Arterioscler Thromb Vasc Biol 25:2020-2030.

Claus SP, Tsang TM, Wang Y, Cloarec O, Skordi E, Martin FP et al. 2008. Systemic multicompartmental effects of the gut microbiome on mouse metabolic phenotypes. Mol Syst Biol 4:1-14.

Coen M, Lenz EM, Nicholson JK, Wilson ID, Pognan F, Lindon JC. 2003. An integrated metabonomic investigation of acetaminophen toxicity in the mouse using NMR spectroscopy. Chem Res Toxicol 16:295-303.

DeVito MJ, Birnbaum LS. 1995. The importance of pharmacokinetics in determining the relative potency of 2,3,7,8-tetrachlorodibenzo-p-dioxin and 2,3,7,8-tetrachlorodibenzofuran. Fundam Appl Toxicol 24:145-148.

Diani-Moore S, Ram P, Li X, Mondal P, Youn DY, Sauve AA et al. 2010. Identification of the aryl hydrocarbon receptor target gene TiPARP as a mediator of suppression of hepatic gluconeogenesis by 2,3,7,8-tetrachlorodibenzo-p-dioxin and of nicotinamide as a corrective agent for this effect. J Biol Chem 285:38801-38810.

DiNatale BC, Schroeder JC, Francey LJ, Kusnadi A, Perdew GH. 2010. Mechanistic insights into the events that lead to synergistic induction of interleukin 6 transcription upon activation of the aryl hydrocarbon receptor and inflammatory signaling. J Biol Chem 285: 24388-24397.

Folch BJ, Lees M, Stanley GHS. 1957. A simple method for the isolation and purification of total lipides from animal J Biol Chem 226: 497-509.

Greenblum S, Turnbaugh PJ, Borenstein E. 2012. Metagenomic systems biology of the human gut microbiome reveals topological shifts associated with obesity and inflammatory bowel disease. Proc Natl Acad Sci USA 109:594-599.

Hautekiet V, Geert V, Marc V, Rony G. 2008. Development of a sanitary risk index for Salmonella seroprevalence in Belgian pig farms. Prev Vet Med 86:75-92.

Hayashi H, Takada T, Suzuki H, Onuki R, Hofmann AF, Sugiyama Y. 2005. Transport by vesicles of glycine- and taurine-conjugated bile salts and taurolithocholate 3-sulfate: a comparison of human BSEP with rat Bsep. Biochim Biophys Acta 1738:54-62.

Hooper LV, Midtvedt T, Gordon JI. 2002. How host-microbial interactions shape the nutrient environment of the mammalian intestine. Annu Rev Nutr 22:283-307.

Hooper LV, Stappenbeck TS, Hong CV, Gordon JI. 2003. Angiogenins: a new class of microbicidal proteins involved in innate immunity. Nat Immunol 4:269-273.

Howell G, Mangum L. 2011. Exposure to bioaccumulative organochlorine compounds alters adipogenesis, fatty acid uptake, and adipokine production in NIH3T3-L1 cells. Toxicol in vitro 25:394-402.

Ivanov II, Atarashi K, Manel N, Brodie EL, Shima T, Karaoz U et al. 2009. Induction of intestinal Th17 cells by segmented filamentous bacteria. Cell 139:485-498.

Jaaskelainen T, Paananen J, Lindstrom J, Eriksson JG, Tuomilehto J, Uusitupa M. 2013. Genetic predisposition to obesity and lifestyle factors--the combined analyses of twenty-six known BMI- and fourteen known waist:hip ratio (WHR)-associated variants in the Finnish Diabetes Prevention Study. Br J Nutr 110:1856-1865.

Jiang CT, Xie C, Li F, Zhang LM, Nichols RG, Krausz1 KW, Cai JW, Qi YP, Fang ZZ, Takahashi S, Tanaka NK, Desai D, Amin SG, Albert I, Patterson AD, Gonzalez1 FJ. 2015. Intestinal farnesoid X receptor signaling promotes nonalcoholic fatty liver disease. J Clin Invest 125:386-402.

Jin UH, Lee SO, Sridharan G, Lee K, Davidson LA, Jayaraman A et al. 2014. Microbiome-derived Tryptophan Metabolites and Their Aryl Hydrocarbon Receptor-Dependent Agonist and Antagonist Activities. Mol Pharmacol 85:777-788.

Jones KC, Bennett BG. 1989. Human exposure to environmental polychlorinated dibenzo-p-dioxins and dibenzofurans: an exposure commitment assessment for 2,3,7,8-TCDD. Sci Total Environ 78:99-116.

Lee DH, Porta M, Jacobs DR Jr, Vandenberg LN. 2014. Chlorinated Persistent Organic Pollutants, Obesity, and Type 2 Diabetes. Endoc Rev er20131084.

Li F, Jiang C, Krausz KW, Li Y, Albert I, Hao H et al. 2013. Microbiome remodelling leads to inhibition of intestinal farnesoid X receptor signalling and decreased obesity. Nat Comm 4: 2384.

Lin RS, Lee FY, Lee SD, Tsai YT, Lin HC, Lu RH et al. 1995. Endotoxemia in patients with chronic liver diseases: relationship to severity of liver diseases, presence of esophageal varices, and hyperdynamic circulation. J Hepatol 22:165-172.

Macpherson AJ, Geuking MB, McCoy KD. 2012. Homeland security: IgA immunity at the frontiers of the body. Trends Immunol 33:160-167.

Maher JM, Cheng X, Slitt, AL, Dieter MZ, Klaassen CD. 2005. Induction of the multidrug resistance-associated protein family of transporters by chemical activators of receptor-mediated pathways in mouse liver. Drug Metab Dispos 33:956-962.

Marshall NB, Kerkvliet NI. 2010. Dioxin and immune regulation: emerging role of aryl hydrocarbon receptor in the generation of regulatory T cells. Ann N Y Acad Sci 1183:25-37.

Mathis D, Benoist C. 2012. The influence of the microbiota on type-1 diabetes: on the threshold of a leap forward in our understanding. Immunol Rev 245:239-249.

Matsubara T, Tanaka N, Krausz KW, Manna SK, Kang DW, Anderson ER et al. 2012. Metabolomics identifies an inflammatory cascade involved in dioxin- and diet-induced steatohepatitis. Cell Metab 16:634-644.

Maurice CF, Haiser HJ, Turnbaugh PJ. 2013. Xenobiotics shape the physiology and gene expression of the active human gut microbiome. Cell 152:39-50.

Mazmanian SK, Liu CH, Tzianabos AO, Kasper DL. 2005. An immunomodulatory molecule of symbiotic bacteria directs maturation of the host immune system. Cell 122:107-118.

Michele C, John H, Paola B, Dino V, Girolamo C. 2010. Morphology of segmented filamentous bacteria and their patterns of contact with the follicle-associated epithelium of the mouse terminal ileum. Gut Microbes 1: 367-372.

Michelle MA, Claudia YD, Timothy RZ. 2013. TCDD-elicited effects on liver, serum, and adipose lipid composition in C57BL/6 Mice. Toxicol Sci 131: 108-115.

Monteleone I, MacDonald TT, Pallone F, Monteleone G. 2012. The aryl hydrocarbon receptor in inflammatory bowel disease: linking the environment to disease pathogenesis. Curr Opin Gastroenterol 28:310-313.

Monteleone I, Pallone F, Monteleone G. 2013. Aryl hydrocarbon receptor and colitis. Semin Immunopathol 35:671-675.

Myre M, Imbeault P. 2014. Persistent organic pollutants meet adipose tissue hypoxia: does cross-talk contribute to inflammation during obesity? Obes Rev 15:19-28.

Nagalingam NA, Lynch SV. 2012. Role of the microbiota in inflammatory bowel diseases. Inflamm Bowel Dis 18:968-984.

Nicholson JK, Holmes E, Kinross J, Burcelin R, Gibson G, Jia W et al. 2012. Host-gut microbiota metabolic interactions. Science 336:1262-1267.

Ozeki J, Uno S, Ogura M, Choi M, Maeda T, Sakurai K et al. 2011. Aryl hydrocarbon receptor ligand 2,3,7,8-tetrachlorodibenzo-p-dioxin enhances liver damage in bile duct-ligated mice. Toxicol 280:10-17.

Peterson DA, McNulty NP, Guruge JL, Gordon JI. 2007. IgA response to symbiotic bacteria as a mediator of gut homeostasis. Cell Host Microbe 2:328-339.

Ren A, Qiu X, Jin L, Ma J, Li Z, Zhang L et al. 2011. Association of selected persistent organic pollutants in the placenta with the risk of neural tube defects. *Proc Natl Acad Sci USA* 108: 12770-12775.

Russell JB. 1985. Fermentation of Cellodextrins by Cellulolytic and Noncellulolytic Rumen Bacteria. Appl Environ Microb 49:572-576.

Said EA, Dupuy FP, Trautmann L, Zhang Y, Shi Y, El-Far M et al. 2010. Programmed death-1-induced interleukin-10 production by monocytes impairs CD4+ T cell activation during HIV infection. Nat Med 16:452-459.

Sayin SI, Wahlstrom A, Felin J, Jantti S, Marschall HU, Bamberg K et al. 2013. Gut microbiota regulates bile acid metabolism by reducing the levels of tauro-beta-muricholic acid, a naturally occurring FXR antagonist. Cell Metab 17:225-235.

Schloss PD, Westcott SL, Ryabin T, Hall JR, Hartmann M, Hollister EB, et al. 2009. Introducing mothur: Open-source, platform-independent, community-supported software for describing and comparing microbial communities. Appl Environ Microbiol 75:7537-7541.

Schwiertz A, Taras D, Schafer K, Beijer S, Bos NA, Donus C et al. 2010. Microbiota and SCFA in lean and overweight healthy subjects. Obesity 18:190-195.

Shin Y, Tze ML, Koji A, Hiroaki K, Seidai S, Seiichit al. 2013. Obesity-induced gut microbial metabolite promotes liver cancer through senescence secretome. Nature 499: 97–101.

Snedeker SM, Hay AG. 2012. Do interactions between gut ecology and environmental chemicals contribute to obesity and diabetes? Environ Health Perspect 120:332-339.

Stappenbeck TS, Hooper LV, Gordon JI. 2002. Developmental regulation of intestinal angiogenesis by indigenous microbes via Paneth cells. Proc Natl Acad Sci USA 99:15451-15455.

Tadashi N, Atsushi Y, Sumiko O. 2011. A survey of dietary intake of plychlorinated dibenzo-*p*-dioxins, polychlorinated dibenzofurans, and dioxin-like coplanar polychlorinated biphenyls from food during 2000-2002 in Osaka city, Japan. Arch Environ Contam Toxicol 60:543-555.

Tian Y, Zhang L, Wang Y, Tang H. 2012. Age-related topographical metabolic signatures for the rat gastrointestinal contents. J Proteome Res 11:1397-1411.

Tremaroli V, Backhed F. 2012. Functional interactions between the gut microbiota and host metabolism. Nature 489:242-249.

Assessment of the health risk of dioxins: re-evaluation of the TDI, WHO Consultation May 25-29, 1998, Geneva, Switzerland. Availale: http://www.who.int/ipcs/publications/en/exe-sum-final.pdf [accessed February 2015].

Wu JF, An YP, Yao JW, Wang YL, Tang HR. 2010. An optimised sample preparation method for NMR-based faecal metabonomic analysis. Analyst 135:1023-1030.

Xun L, Topp E, Orser CS. 1992. Glutathione is the reducing agent for the reductive dehalogenation of tetrachloro-p-hydroquinone by extracts from a Flavobacterium sp. Biochem Biophys Res Commun 182:361-366.

Yap IK, Clayton TA, Tang H, Everett JR, Hanton G, Provost JP et al. 2006. An integrated metabonomic approach to describe temporal metabolic disregulation induced in the rat by the model hepatotoxin allyl formate. J Proteome Res 5:2675-2684.

Zelante T, Iannitti RG, Cunha C, De Luca A, Giovannini G, Pieraccini G et al. 2013. Tryptophan catabolites from microbiota engage aryl hydrocarbon receptor and balance mucosal reactivity via interleukin-22. Immun 39:372-385.

Zhang L, Ye Y, An Y, Tian Y, Wang Y, Tang H. 2011. Systems responses of rats to aflatoxin B1 exposure revealed with metabonomic changes in multiple biological matrices. J Proteome Res 10:614-623.

Figure Legends

Figure 1. Xenobiotic responses of mice to dietary TCDF. Light microscopic examination of the liver from *Ahr*$^{+/+}$ (A) and *Ahr*$^{-/-}$ (B) vehicle and TCDF-treated mice (24 μg/kg). Arrows indicate inflammatory foci. Scale bars = 200 μm. (C) Serum ALT and ALP concentration of *Ahr*$^{+/+}$ and *Ahr*$^{-/-}$ vehicle and TCDF-treated mice. (D) Percent change in body weight of mice recorded every other day during adaptation and treatment period. (E) *Cyp1a1, Cyp1a2, Cyp2e1* and *Cyp2a1* expression in the liver and intestinal *Cyp1a1* mRNA expression. (F) *Cyp1a1* and *Cyp1a2* mRNA expression in the liver of *Ahr*$^{-/-}$ vehicle and TCDF-treated *Ahr*$^{-/-}$ mice. Data are presented as mean ± s. d, n = 5 or 6 per group; *$p < 0.05$, **$p < 0.01$, NS means no significance, two-tailed Student's *t*-test or Mann Whitney.

Figure 2. Effects of dietary TCDF on the morphology, population, and composition of gut microbiota. Mice were treated for 5 days with dietary TCDF (24 μg/kg) and sampled on day 7. (A) Weighted UniFrac principal coordinate analysis of the total population of gut microbiome of cecal content from *Ahr*$^{+/+}$ and *Ahr*$^{-/-}$ mice. (B) 16S rRNA gene sequencing analysis at the phylum level of the cecal content. (C) 16S rRNA gene sequencing analysis at the class and genus levels of cecal contents. (D) Scanning electron microscopy imagines (50 μm) of ileum and (E) qPCR analysis of ileum SFB from wild type and *Ahr*$^{-/-}$ mice. Data are presented as mean ± s. d, n = 5 or 6 per group; NS means no significance, two-tailed Student's *t*-test or Mann Whitney.

Figure 3. Dietary TCDF and AHR-dependent inflammation. (A) qPCR analysis of mRNA levels of inflammatory cytokine (*IL-1β, TNF-α, IL-10, Saa1* and *Saa3*) expression in the ileum of *Ahr*$^{+/+}$ vehicle- and TCDF-treated *Ahr*$^{+/+}$ mice. (B) *IL-1β* and *Tnf-α* expression in the ileum of *Ahr*$^{-/-}$ vehicle and TCDF-treated *Ahr*$^{-/-}$ mice. (C) qPCR analysis of mRNA levels of *Lcn-2* expression in the ileum of *Ahr*$^{+/+}$ and *Ahr*$^{-/-}$ vehicle and TCDF-treated mice. Quantification of fecal LCN2 (D) and IgA (G) by ELISA. (E) qPCR analysis of mRNA levels of *Myosin Vb* and *Ptprh* in the ileum after TCDF treatment. (F) Quantification of serum LPS. Data are presented as mean ± s. d, n = 5 per group; *$p < 0.05$, **$p < 0.01$, ***$p < 0.001$, NS means no significance, two-tailed Student's *t*-test.

Figure 4. Dietary TCDF and bile acid metabolism. (A-D) Quantification of specific bile acids levels in intestinal tissue and feces throughout the enterohepatic circulation of vehicle and TCDF-treated (24 μg/kg, $Ahr^{+/+}$ mice). (E) Quantification of total bile acids in liver, intestine, cecum and feces. The bile acid profile in the small intestine shows the data from jejunum segment. QPCR analysis of *Fgf15*, *Fxr* and *Shp* mRNAs in the ileum (F) and *Fxr* and *Shp* mRNA expression in the liver (G) of $Ahr^{+/+}$ and $Ahr^{-/-}$ vehicle and TCDF-treated mice. (H) QPCR analysis of *Cyp7a1*, *Cyp8b1*, *Cyp27a1*, *Akr1d1* and *Cyp7b1* mRNAs in the liver. (I-K) mRNA encoding bile acid transporters involved in taurine biosynthesis and bile acid conjugation in the ileum (I), mRNA encoding bile acid transporters in the distal liver (J) and ileum (K) of vehicle- and TCDF-treated mice (24 μg/kg, $Ahr^{+/+}$ mice). Data are presented as mean ± s. d, n = 6 per group; *$p < 0.05$, **$p < 0.01$, two-tailed Student's *t*-test. CA, cholic acid; LCA, lithocholic acid; UDCA, ursodeoxycholic acid; CDCA, chenodeoxycholic acid; DCA, deoxycholic acid; MCA, muricholic acid; G, glycine-conjugated; T, taurine-conjugated species. See also Supplemental Material Table S1 and S2.

Figure 5. Effects of dietary TCDF on host metabolism and the bacterial fermentation process. OPLS-DA scores (left) and coefficient-coded loadings plots for the models (right) from NMR spectra of aqueous fecal (A), cecal content (B), and liver extracts (C) discriminating between the vehicle (black dots) and TCDF-treated mice (red squares). These models are cross-validated with CV-ANOVA, $p = 1.64\times10^{-3}$, $p = 0.033$ and $p = 0.0018$; corresponding to feces, cecal content and liver of mice after vehicle and TCDF exposure (24 μg/kg), respectively. Metabolites assignment is shown in Supplemental Material Figure S5 and Table S4 and correlation coefficient values for the significantly changed metabolites are shown in Supplemental Material Table S3.

Figure 1.

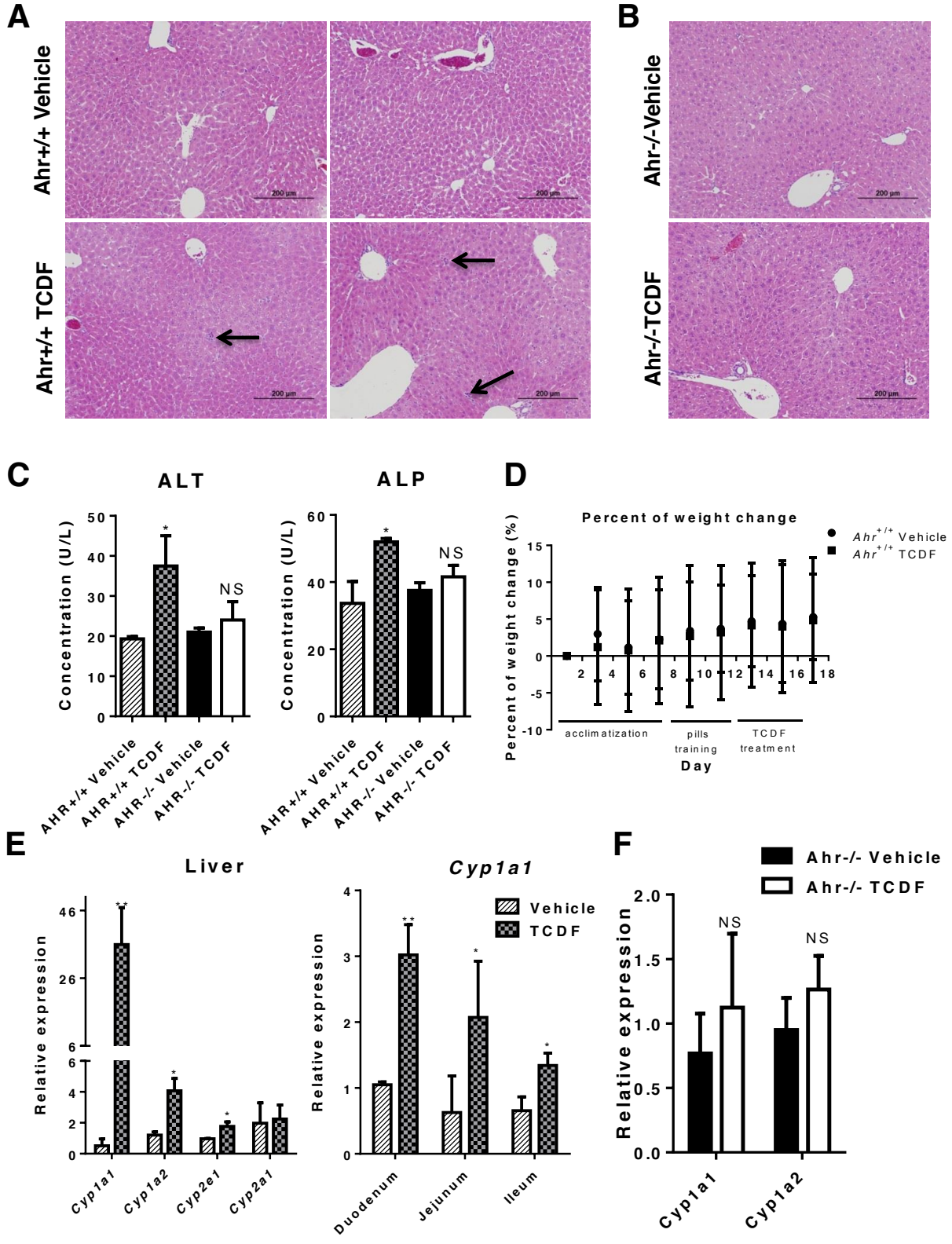
A
Ahr+/+ Vehicle
Ahr+/+ TCDF
200 μm
B
Ahr-/-Vehicle
Ahr-/-TCDF
200 μm
C
ALT
Concentration (U/L)
NS
AHR+/+ Vehicle
AHR+/+ TCDF
AHR-/- Vehicle
AHR-/- TCDF
ALP
Concentration (U/L)
NS
D
Percent of weight change
Percent of weight change (%)
Ahr+/+ Vehicle
Ahr+/+ TCDF
acclimatization
pills training
TCDF treatment
Day
E
Liver
Relative expression
Cyp1a1
Cyp1a2
Cyp2e1
Cyp2a1
Cyp1a1
Vehicle
TCDF
Duodenum
Jejunum
Ileum
F
Ahr-/- Vehicle
Ahr-/- TCDF
Relative expression
NS
NS
Cyp1a1
Cyp1a2

Figure 2.

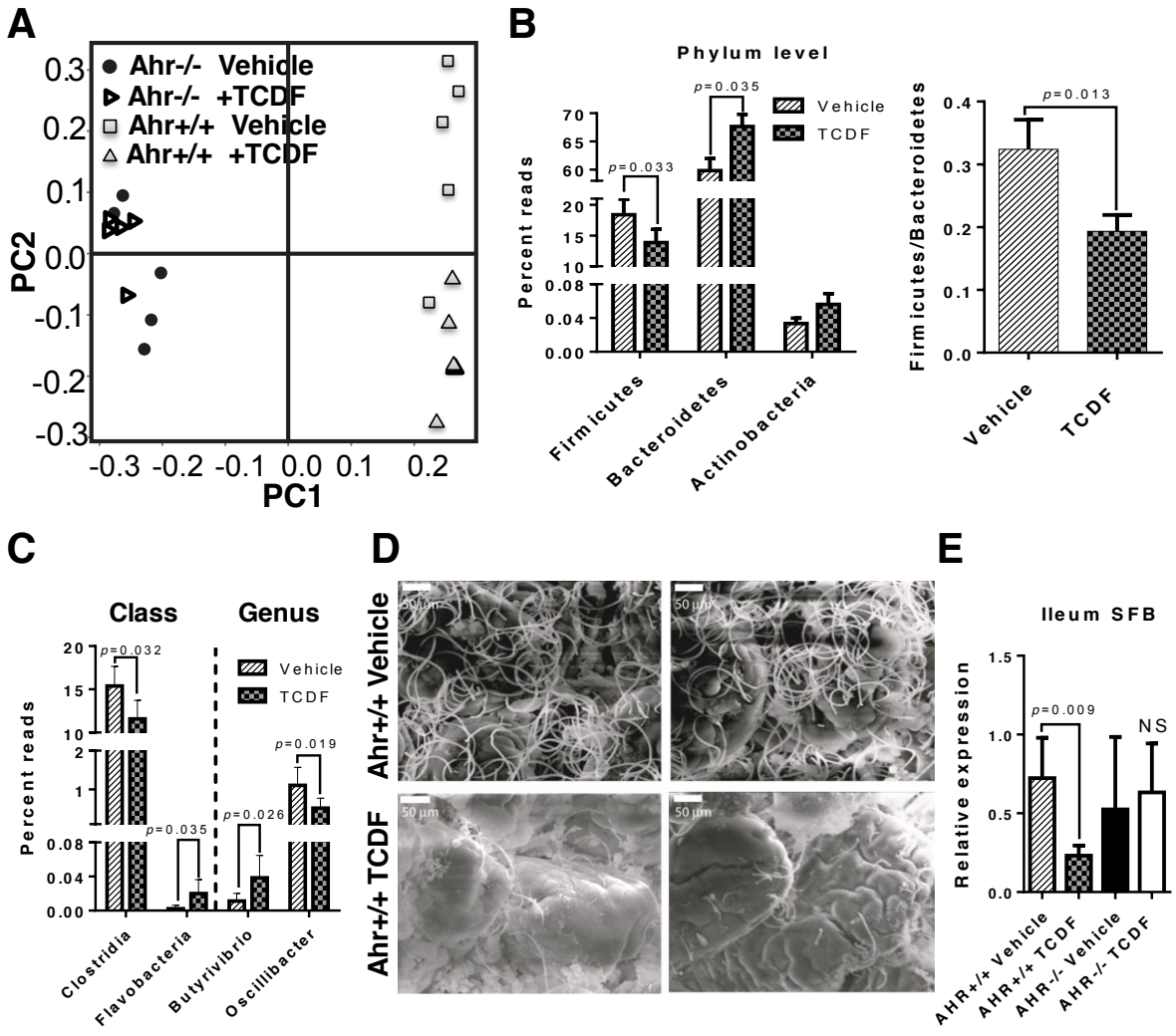
A
Ahr-/- Vehicle
Ahr-/- +TCDF
Ahr+/+ Vehicle
Ahr+/+ +TCDF
PC1
PC2
B
Phylum level
Vehicle
TCDF
Percent reads
p=0.033
p=0.035
Firmicutes
Bacteroidetes
Actinobacteria
Firmicutes/Bacteroidetes
p=0.013
Vehicle
TCDF
C
Class
Genus
Vehicle
TCDF
Percent reads
p=0.032
p=0.035
p=0.026
p=0.019
Clostridia
Flavobacteria
Butyrivibrio
Oscillibacter
D
Ahr+/+ Vehicle
Ahr+/+ TCDF
50 µm
E
Ileum SFB
Relative expression
p=0.009
NS
AHR+/+ Vehicle
AHR+/+ TCDF
AHR-/- Vehicle
AHR-/- TCDF

Figure 3.

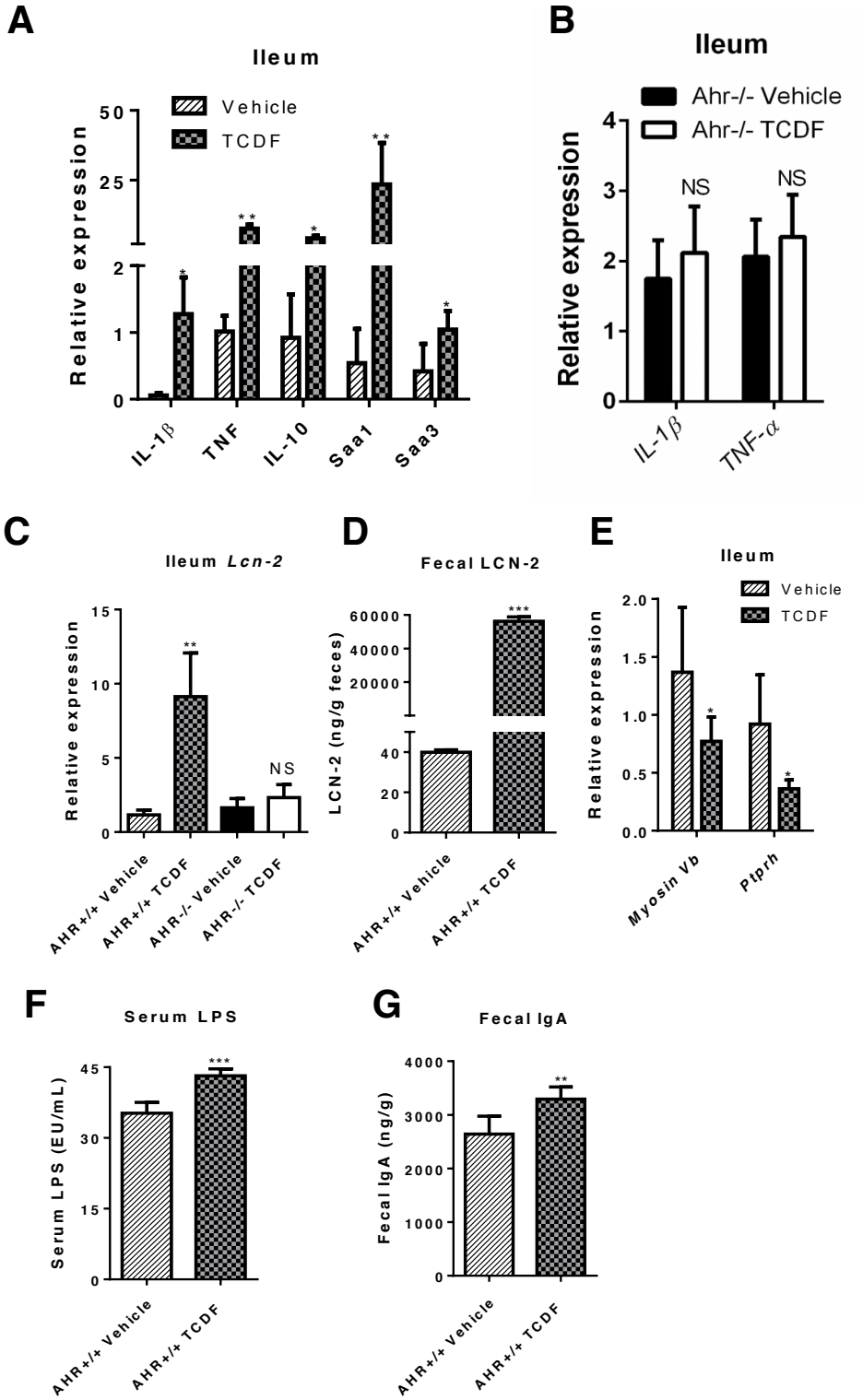
A
Ileum
Vehicle
TCDF
Relative expression
IL-1β
TNF
IL-10
Saa1
Saa3
B
Ileum
Ahr-/- Vehicle
Ahr-/- TCDF
NS
NS
Relative expression
IL-1β
TNF-α
C
Ileum Lcn-2
Relative expression
NS
AHR+/+ Vehicle
AHR+/+ TCDF
AHR-/- Vehicle
AHR-/- TCDF
D
Fecal LCN-2
LCN-2 (ng/g feces)
AHR+/+ Vehicle
AHR+/+ TCDF
E
Ileum
Vehicle
TCDF
Relative expression
Myosin Vb
Ptprh
F
Serum LPS
Serum LPS (EU/mL)
AHR+/+ Vehicle
AHR+/+ TCDF
G
Fecal IgA
Fecal IgA (ng/g)
AHR+/+ Vehicle
AHR+/+ TCDF

Figure 4.

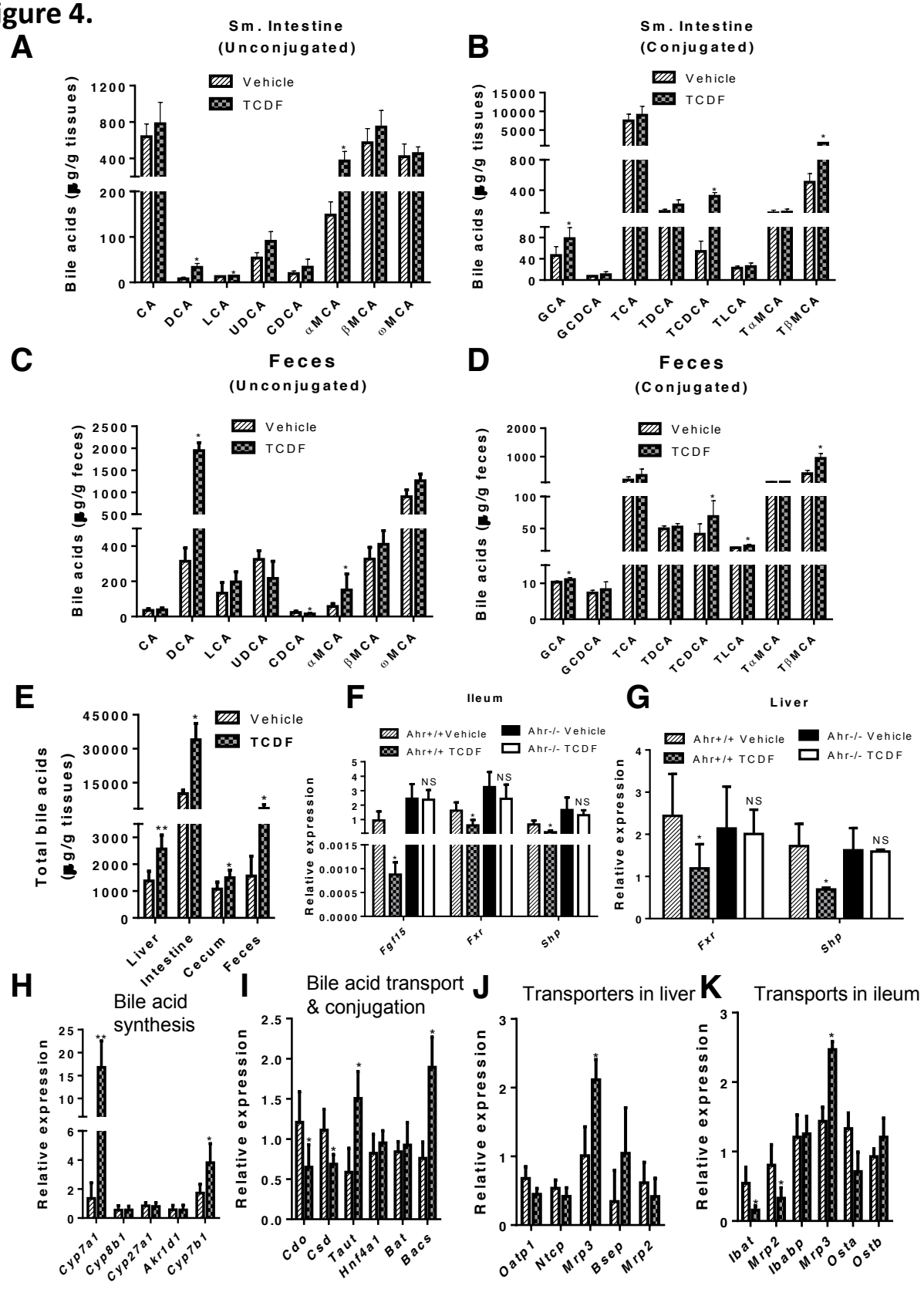
A
Sm. Intestine
(Unconjugated)
Vehicle
TCDF
Bile acids (μg/g tissues)
CA
DCA
LCA
UDCA
CDCA
αMCA
βMCA
ωMCA
B
Sm. Intestine
(Conjugated)
GCA
GCDCA
TCA
TDCA
TCDCA
TLCA
TαMCA
TβMCA
C
Feces
(Unconjugated)
Bile acids (μg/g feces)
D
Feces
(Conjugated)
E
Total bile acids (μg/g tissues)
Liver
Intestine
Cecum
Feces
F
Ileum
Ahr+/+Vehicle
Ahr+/+ TCDF
Ahr-/- Vehicle
Ahr-/- TCDF
Relative expression
NS
Fgf15
Fxr
Shp
G
Liver
H
Bile acid synthesis
Cyp7a1
Cyp8b1
Cyp27a1
Akr1d1
Cyp7b1
I
Bile acid transport & conjugation
Cdo
Csd
Taut
Hnf4a1
Bat
Bacs
J
Transporters in liver
Oatp1
Ntcp
Mrp3
Bsep
Mrp2
K
Transports in ileum
Ibat
Mrp2
Ibabp
Mrp3
Osta
Ostb

Figure 5.

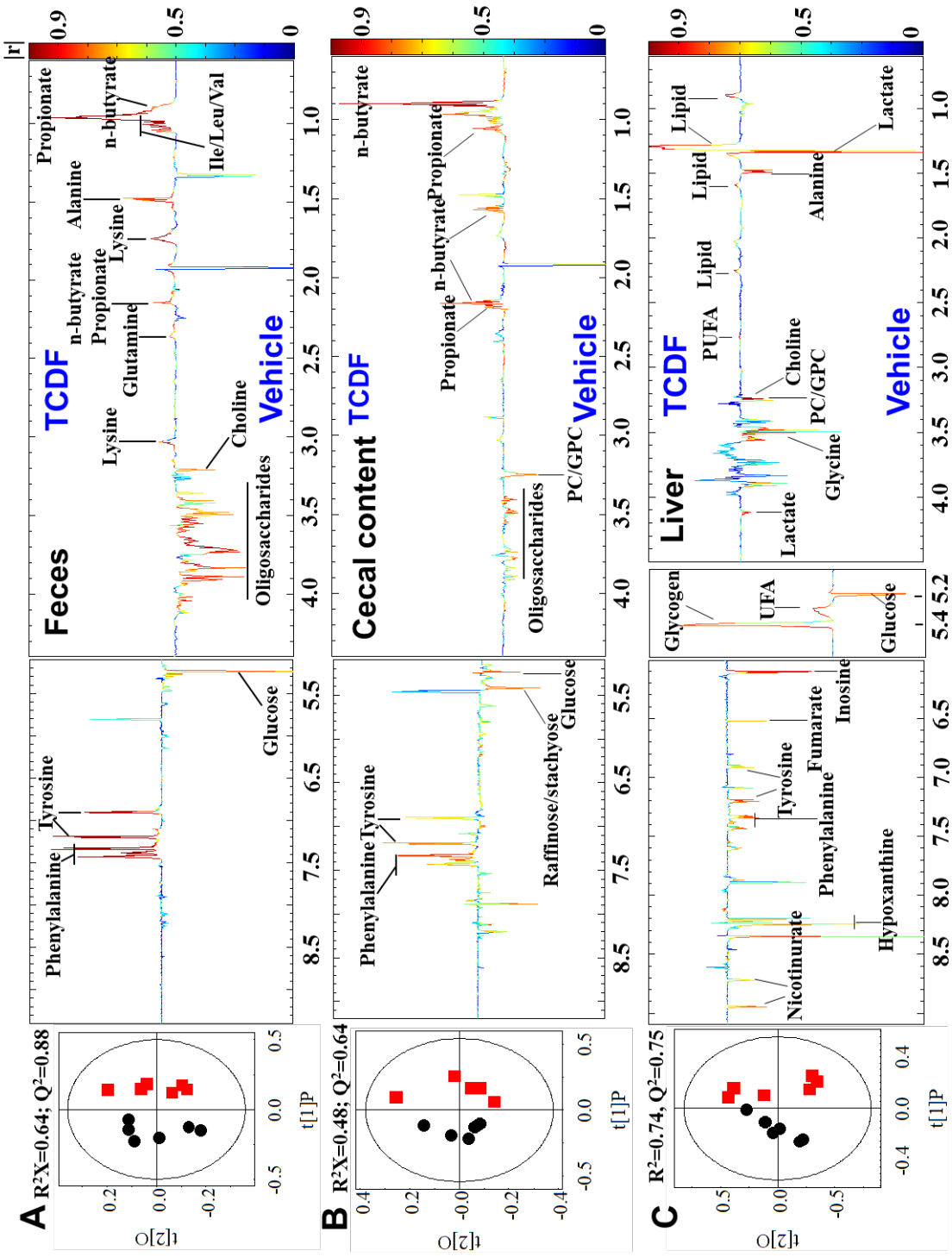
A
R²X=0.64; Q²=0.88
Feces
TCDF
Vehicle
Propionate
n-butyrate
Alanine
Lysine
Glutamine
Ile/Leu/Val
Choline
Oligosaccharides
Phenylalanine
Tyrosine
Glucose
|r|
B
R²X=0.48; Q²=0.64
Cecal content
TCDF
Vehicle
Raffinose/stachyose
PC/GPC
C
R²=0.74, Q²=0.75
Liver
TCDF
Vehicle
Lipid
PUFA
Choline
PC/GPC
Glycine
Lactate
Glycogen
UFA
Nicotinurate
Fumarate
Inosine
Hypoxanthine
t[1]P
t[2]O